Sādhanā Vol. 41, No. 11, November 2016, pp. 1311–1320
DOI 10.1007/s12046-016-0556-x

Transient pressure measurements at part load operating condition of a high head model Francis turbine

RAHUL GOYAL[1], CHIRAG TRIVEDI[2], B K GANDHI[1,*], MICHEL J CERVANTES[2,3] and OLE G DAHLHAUG[2]

[1]Department of Mechanical and Industrial Engineering, Indian Institute of Technology Roorkee, Roorkee 247667, India
[2]Water Power Laboratory, Department of Energy and Process Engineering, Norwegian University of Science and Technology, Trondheim, Norway
[3]Division of Fluid and Experimental Mechanics, Department of Engineering Sciences and Mathematics, Luleå University of Technology, Luleå, Sweden
e-mail: bkgmefme@iitr.ernet.in

MS received 8 May 2015; revised 31 January 2016; accepted 23 May 2016

Abstract. Hydraulic turbines are operating at part load conditions depending on availability of hydraulic energy or to meet the grid requirements. The turbine experiences more fatigue during the part load operating conditions due to flow phenomena such as vortex breakdown in the draft tube and flow instability in the runner. The present paper focuses on the investigation of a high head model Francis turbine operating at 50% load. Pressure measurements have been carried out experimentally on a model Francis turbine. Total six pressure sensors were mounted inside the turbine and other two pressure sensors were mounted at the turbine inlet pipe. It is observed that the turbine experiences significant pressure fluctuations at the vaneless space and the runner. Moreover, a standing wave is observed between the pressure tank outlet and the turbine inlet. Analysis of the data acquired by the pressure sensors mounted in the draft tube showed the presence of vortex breakdown co-rotating with the runner. The detailed analysis showed the rotating and plunging components of the vortex breakdown. The influence of the rotating component was observed in the entire hydraulic circuit including distributor and turbine inlet but not the plunging one.

Keywords. Francis turbine; pressure fluctuations; rotor stator interaction; vortex rope; runner.

1. Introduction

Hydraulic turbines are normally designed to operate at the best efficiency point (BEP); however, they need to be operated at part load conditions to meet either available hydraulic energy or demand of market. The turbine experiences unstable flow conditions during the operation away from BEP due to unfavorable pressure loading on the runner blades [1]. Upstream of the runner, the flow becomes unstable due to high amplitude pressure fluctuations caused by the rotor–stator interaction (RSI). Similarly, the flow at the runner outlet becomes largely separated due to vortex breakdown affecting stable operation of the turbine. Moreover, asymmetric pressure loading of the runner blades during part load operation increases blade fatigue [2]. When a turbine is operated at part load, it experiences high vibrations which may lead to resonance in some cases [2–5]. Experimental and numerical investigations on a Francis turbine showed that the flow conditions deteriorate for turbine operation away from BEP due to the complex interaction between the guide vanes and the runner blades, asymmetric loading on the blades, vortex breakdown in the draft tube and standing waves in the hydraulic circuit [6].

The flow field leaving the guide vanes row is normally characterized by its complexity caused by the RSI since blades are rotating and the guide vanes are stationary. When a blade passes in front of a guide vane, it receives a hydrodynamic force. The interaction develops unsteady pressure and velocity field at the runner inlet, i.e., vaneless space [7]. During the interaction, a pressure wave is generally developed and propagated at the speed of sound generating pressure fluctuations. Since the turbine runner is operated at synchronous speed, cyclic interactions between the blades and the guide vanes are developed inducing fluctuations in the hydraulic torque [8, 9]. Unsteady pressure fluctuations and large variation of velocity at the runner inlet were attributed to the torque fluctuations specifically at part load operation [10].

*For correspondence

Trailing edge vortical flow leaving the guide vanes enters the rotating domain during the turbine operation. The flow leaving the runner blade and trailing edge swirl causes largely separated flow in the draft tube. At BEP, the tangential velocity component at the runner outlet is relatively small and thus the turbine operates without vortex breakdown under stable condition. However, away from the BEP, the flow leaving the runner has a large tangential component. In a Francis turbine, the fixed relative exit angle of the runner blade is designed for an optimum discharge condition. At low discharge, part load, the relative velocity angle remains nearly the same, but the absolute velocity angle induces a residual swirl in the direction of the runner rotation. Whereas at high discharge, above BEP flow rate, the direction of the swirl is opposite to the runner rotation. Thus the dynamic stability of the turbine is significantly affected during part load operation [11]. The experimental measurements on a Francis turbine showed that high pressure amplitudes in the draft tube induce excitation and large vibrations in the turbine [12]. The system vibration frequency is associated with the vortex rope frequency of 0.2–0.4 times of runner frequency which may cause resonance in the hydraulic structure [13, 14].

Further, analysis of RSI and vortex rope showed that there may be development of standing pressure waves, at specific frequencies. The occurrence of the standing wave is dependent on the travel time of the pressure wave propagation [15]. One-dimensional model was used by Fischer *et al* [16] to show a link between the standing wave in the spiral casing due to RSI and the diametrical pressure mode rotating in the vaneless space.

Bosioc *et al* [17] decomposed pressure signals obtained from two radially opposite mounted pressure sensors in the draft tube cone to determine the rotating and plunging components of the vortex rope. The addition of the two signals, the symmetric component, is called as plunging component whereas the difference of the two signals is termed as the rotating component. They observed that the rotating component is dominated when there is no water jet injection whereas the plunging component is dominated for 14% water jet injection in the draft tube.

It is seen that the unsteadiness at the part load operating conditions hinders the smooth operation of the turbine. Fatigue to the turbine blades is relatively high. Present trend of the hydraulic turbine operation frequently forces to operate it away from the BEP. Moreover, during the winter season, hydraulic turbine operates at part load ($\sim$50% load) conditions to avoid freezing damage inside the hydraulic systems and keep water flowing through the systems. The developed power at this load is used for heating of the components inside the power plant as well as piping systems. The main focus of this work is to investigate the pressure loading inside the turbine at a similar load. No measurements have been reported in the literature at this operating load, specifically pressure measurements in the runner and vaneless space. This measurement enabled us to understand the pressure field during such conditions. Average and instantaneous pressure loading on the blades, vaneless space, and draft tube was investigated. The data acquired by the pressure sensors at different locations revealed useful information regarding amplitude of the unsteady pressure fluctuations due to RSI and vortex breakdown at the runner downstream.

2. Model test rig and measurement programme

The model turbine, used in the present work, is installed at the Waterpower laboratory, Norwegian University of Science and Technology (NTNU), Norway. The model turbine is a 1:5.1 scale model of the prototype. The prototype turbine (head = 377 m, power = 110 MW, and runner diameter = 1.779 m, discharge = 31 $m^3 s^{-1}$, specific speed = 0.27) is in operation at the Tokke power plant, Norway. A schematic of the test rig is presented in figure 1. Water from the basement was pumped to the overhead tank which flowed down to the upstream pressure tank connected to the turbine inlet. A uniform level of the water was maintained in the overhead tank. The draft tube was connected to the downstream tank, which was open to the air, and the water was released back to the large basement. The model is integrated with 14 stay vanes conjoined inside the spiral casing, 28 guide vanes, a runner with 15 splitters and 15 full length blades, and an elbow-type draft tube. At the inlet pipeline, two pressure transmitters, PTX1 and PTX2 were mounted at 4.87 m and 0.87 m upstream of the turbine inlet, respectively. A magnetic flow meter was used to measure the turbine discharge and a differential pressure transducer was used to acquire the pressure difference across the turbine.

Calibration of the mounted instruments and sensors were carried out before the steady state measurements. Figure 2 shows the locations of the six miniature pressure sensors mounted inside the turbine. One of the sensors was mounted in the vaneless space (VL01) to measure the pressure at the runner inlet; two sensors were mounted on the pressure side of the blade (P41 and P71) and one sensor was mounted on the suction side of the blade (S51). The remaining two sensors, DT11 and DT21, were mounted in the draft tube cone at the same elevation and radially 180° apart. The calibration and uncertainty analysis were performed according to the procedure and guidelines available in IEC 60193 [18] and IEC 60041 [19]. The acquired parameters from the instruments were stored in a computer through a Lab-View program. Two acquisitions systems were used – one to acquire the parameters specific to the test rig, which was sampled at 1.45 Hz, and another to acquire the pressure–time signal of the eight pressure sensors at an approximate sampling frequency of 2100 Hz.

The random errors, systematic errors and related uncertainties were estimated using IEC 60193 [18]. The systematic uncertainty in the hydraulic efficiency was

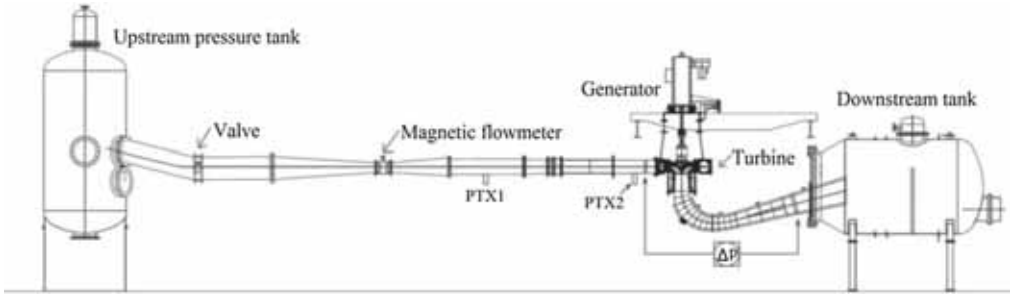

Figure 1. Test rig of the model Francis turbine.

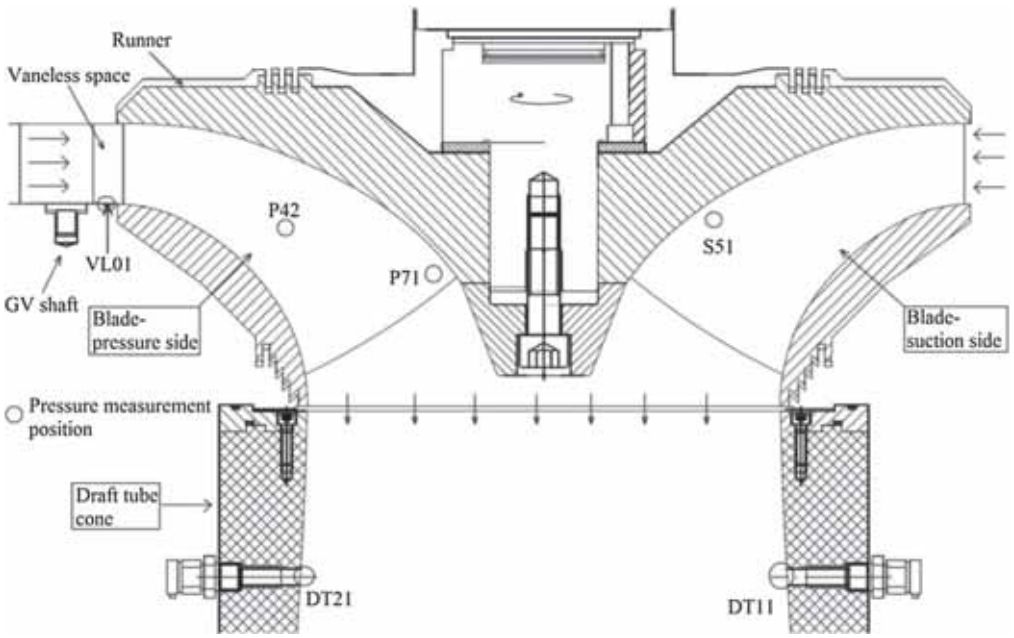

Figure 2. Locations of the pressure sensors – VL01, P42, P71, S51, DT11 and DT21 used for pressure measurements.

estimated by the root-sum-square of all individual uncertainties, namely uncertainties in the discharge $(\delta_Q)_{sys}$, the specific hydraulic energy $(\delta_E)_{sys}$, the torque $(\delta_T)_{sys}$, the angular speed $(\delta_\omega)_{sys}$, and the density of water $(\delta_\rho)_{sys}$. The total uncertainty in evaluation of hydraulic efficiency was estimated as $\pm 0.16\%$ at BEP ($\alpha = 9.8°$, $n_{ED} = 0.18$, $q_{ED} = 0.15$) of the model Francis turbine.

Calibration uncertainty and accuracy of the pressure sensors are shown in table 1. The pressure sensors were calibrated by secondary method. A hydraulic dead weight tester was used as primary calibration device for the pressure transmitters, PTX1, PTX2, and PTX1400. The PTX1400 was used for the calibration of the pressure sensors mounted in the vaneless space (VL01), runner (P42, P71 and S51) and draft tube (DT11 and DT21). The estimated uncertainties were $\leq 0.22\%$, $\leq 0.62\%$, and $\leq 0.45\%$ for S51, P42, and P71 respectively, and $\leq 0.15\%$ for VL01, DT11 and DT21.

The pressure measurements were carried out at the part load operation. The turbine was operated at 50% load for a guide vanes angular position (α) of 6.72° ($q_{ED} = 0.096$ and $n_{ED} = 0.19$). The runner was rotating at a constant rotational frequency of 5.94 Hz. The detailed investigation and analysis of the acquired pressure values at different locations at this operating point are discussed below.

3. Results and discussion

Constant efficiency hill diagram of the model Francis turbine is shown in figure 3 [1]. The maximum hydraulic efficiency (93.4%) was observed at a guide vanes angular position of 9.9°, which is marked as BEP. At BEP, the speed factor (n_{ED}) and discharge factor (q_{ED}) are 0.18 and 0.15, respectively. The operating point selected for the present investigation is marked in figure 3 [1] at a guide

Table 1. Accuracy and calibration uncertainties of the pressure sensors mounted inside the turbine.

Instrument	Accuracy	Uncertainty	Position of installation
Hydraulic dead-weight tester (1–350 bar)	0.008% of actual reading	≤0.01%	Used as a primary calibration device for PTX pressure transmitters
PTX1 (0–250 kPa abs)	0.08% FSBSL	≤0.02%	Turbine inlet pipeline
PTX2 (0–250 kPa abs)	0.08% FSBSL	≤0.03%	Turbine inlet
PTX1400 (0–1000 kPa abs)	±0.15% typical BSL, ±0.25% maximum	≤0.04%	Used as a primary calibration device for Kulite LL080
Miniature pressure sensors, Kulite LL080 (0–350 kPa abs); Bandwidth ≈100 kHz and 300 kHz natural frequency	±0.10% FSBSL, ±0.50% maximum	S51: ≤0.22% P42: ≤0.62% P71: ≤0.45%	Installed on the runner blades
Miniature ruggedized Kulite XTL-190 (0–700 kPa abs) 380 kHz natural frequency	±0.10% FSBSL, ±0.50% maximum	VL01, DT11, DT21: ≤0.15%	Installed in vaneless space (VL01) and draft tube cone (DT11, DT21)

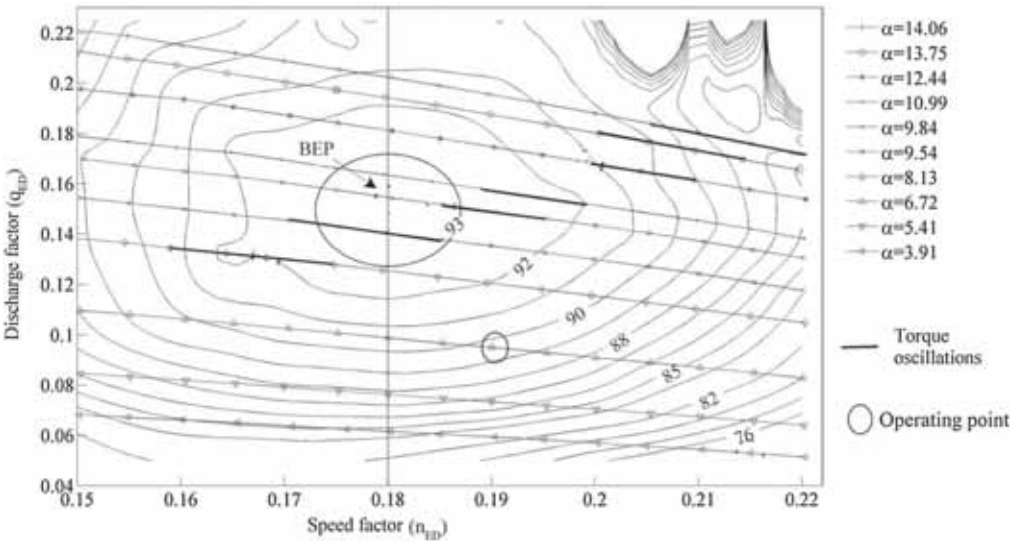

Figure 3. Hill diagram of the high head model Francis turbine [1].

vanes opening of 6.72° at $n_{ED} = 0.19$ and $q_{ED} = 0.096$. At this operating point, the load on the turbine is 50% of the maximum load and the hydraulic efficiency is 89%.

3.1 *Average pressure*

The pressure values were averaged over the length of the acquired signal according to IEC 60193 [18] using the following equation.

$$\overline{X} = \frac{\sum_1^N X_N}{N}. \quad (1)$$

Samples of pressure–time signals were averaged over 50 revolutions of the runner. The averaged pressure values are shown in figure 4. The average pressure at the location PTX1 was 219.0 kPa and 271.4 kPa at PTX2. At the location VL01, located close to the trailing edge of the guide vane, the average pressure was 169.0 kPa. A part of the pressure energy is converted into kinetic energy in the Francis turbine so there is a continuous decrease in pressure values in the runner. The pressure observed at the sensors P42, S51 and P71 was 107.40, 99.50 and 95.80 kPa, respectively. The sensors DT11 and DT21 showed a comparatively high value of the average pressure, namely 102.70 and 102.0 kPa, respectively.

3.2 *Pressure fluctuations*

The pressure fluctuations inside the turbine with respect to the runner angular position have been investigated. The acquired pressure signal ($\tilde{p}$) was subtracted from its mean

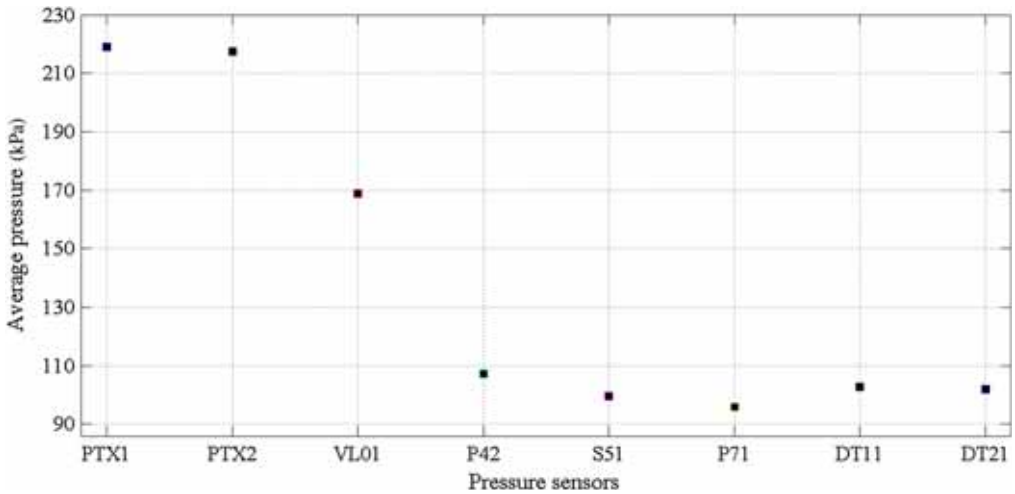

Figure 4. Variation of the average pressure at different locations in the turbine at $Q = 0.1265$ m^3 s^{-1}.

pressure ($\bar{p}$) to obtain the fluctuating pressure (p^*) using the following equation.

$$p^* = \tilde{p} - \bar{p} \text{ (kPa)}. \tag{2}$$

A bandpass filter was designed to filter out the frequencies related to the system excitations and noise as shown in the following equation.

$$H_{BP}(f) = \begin{Bmatrix} 1 & F_{c1} \leq f \leq F_{c2} \\ 0 & \text{otherwise} \end{Bmatrix} \tag{3}$$

where $H_{BP}(f) = H_{LP2}(f) - H_{LP1}(f)$, $H_{LP2}(f)$ and $H_{LP1}(f)$ are low-pass filters with the lower and upper cut-off frequency F_{c1} and F_{c2}, respectively and, f is the frequencies in pressure–time raw signal.

The pressure fluctuations for one complete rotation of the runner at VL01, P42, DT11 and DT21 are presented in figure 5(a–c). The pressure fluctuations at the vaneless space are shown in figure 5(a). At VL01, there are 30 peaks for one runner rotation which correspond to the number of runner blades (splitter + full length blades). The dimensional frequency for this signal is 178.20 Hz which is equal to the runner rotational frequency (5.94 Hz) multiplied by the number of runner blades (30). The maximum amplitude of the fluctuations is ±0.75 kPa. At P42, the signal has 28 peaks for one runner rotation which correspond to the number of guide vanes as shown in figure 5(b). The dimensional frequency for this signal is 166.32 Hz which is equal to the runner rotational frequency (5.94 Hz) multiplied by the number of guide vanes (28). The maximum amplitude of ±1.14 kPa was observed at this location. At DT11 and DT21, 30 peaks were obtained simultaneously at each of the sensors with little variation in amplitudes as shown in figure 5(c). The observed amplitudes were within ±0.08 kPa at these locations.

In Francis turbine when a blade passes in front of a guide vane, it interacts and exchanges momentum, which develops waves in the flowing fluid. The rotor–stator interaction (RSI) frequency depends on three parameters namely, number of guide vanes, number of runner blades and angular speed of the runner. This indicates that at each runner blade/guide vane interaction, a pressure pulse develops. Therefore, the numbers of pressure fluctuation peaks are equal to the number of guide vanes in the runner and the number of runner blades in the stationary domain, i.e., distributor and draft tube as expected.

In order to investigate the dominant frequencies of the pressure fluctuation at different locations, fast Fourier transform (FFT) of the pressure signals has been carried out and presented in the next section.

3.3 *Spectral analysis*

An FFT analysis of the pressure–time data acquired by all eight pressure sensors has been carried out to investigate the frequencies in the turbine at different locations. The different frequencies were analyzed. The frequencies related to flow phenomena were filtered out by designing a cascade of bandpass filters in MATLAB to eliminate the frequencies due to vibration and noise. Figure 6 shows the frequency spectrum of the pressure signals acquired by all the sensors. The x-axis shows the normalized frequency and the y-axis displays the absolute pressure in kPa. The frequencies were normalized using the following equation.

$$f^* = \frac{f}{f_n}[-]. \tag{4}$$

Pressure sensor, PTX1 was mounted near the flow meter and approximately 4.5 m downstream of the water pressure tank. It showed amplitudes of 0.03 and 0.05 kPa for normalized frequency of 2.25 and 4.50, respectively. Similar frequencies were observed at the sensor PTX2, mounted downstream of PTX1. The frequencies are attributed to the

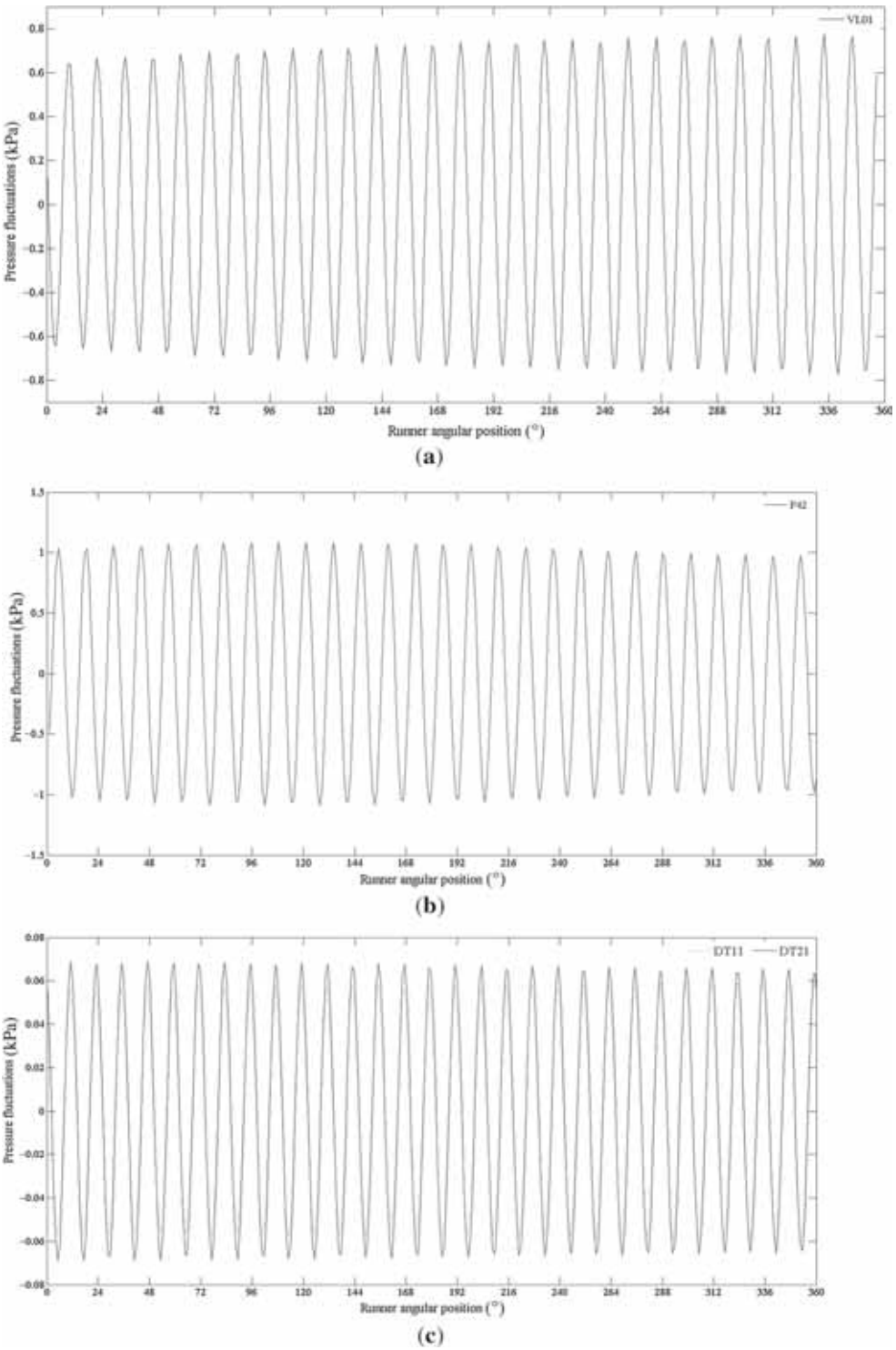

Figure 5. Pressure fluctuation filtered at the RSI frequency for one complete rotation of the runner at (**a**) VL01, (**b**) P42, and (**c**) DT11 and DT21.

standing wave in the pipe and its harmonics. The wavelength (λ) of the standing wave was estimated using the following equation.

$$\lambda = 4L \tag{5}$$

where L is the inlet pipe length from the pressure tank outlet to the nose vane of the spiral casing. A wave length of 55 m was obtained.

Assuming a sound velocity in water of 1440 m s^{-1}, a frequency of 2.25 was obtained similar to the one obtained

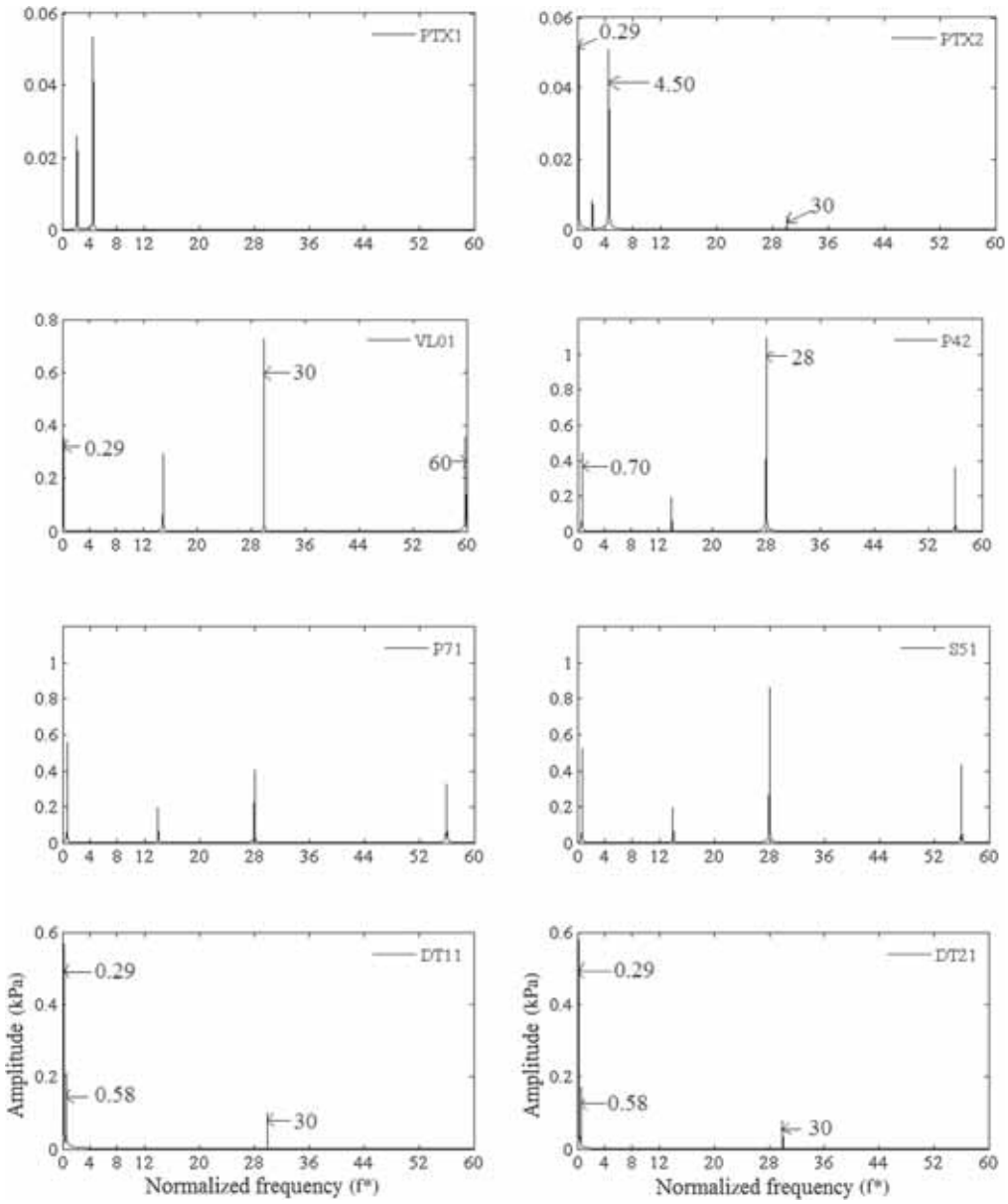

Figure 6. Frequency spectrum of the pressure–time signals.

in the spectral analysis. At the location PTX2, amplitude of 0.003 and 0.05 kPa was observed for normalized frequency of 30 and 0.29, respectively. These frequencies correspond to the RSI and the vortex breakdown frequencies, respectively. The same frequencies were observed at PTX2 but not at PTX1 which is located upstream of PTX2 and close to the pressure tank. Thus, the influence of RSI and the vortex breakdown are damped out as one travels upstream of flow.

Spectrum analysis of the pressure signal at VL01 in figure 6 showed that the dominant amplitude of 0.75 kPa is observed at the normalized frequency of 30, i.e., the blade passing frequency. The second and half harmonic of the blade passing frequency were also observed. Another low amplitude of 0.33 kPa was observed at a normalized frequency of 0.29 which is attributed to the vortex breakdown. Many researchers [20] observed that the vortex breakdown frequency is 0.2–0.4 times of the runner frequency, and the rotating and plunging components of the vortex rope are typically assimilated to the form of vortex breakdown. The sensors mounted on the blade surface at P42, P71, and S51 showed a normalized fundamental frequency of 28, which is related to the guide vanes passing frequency. Low pressure amplitudes were also observed at the second (56) and half harmonics (14) of the guide vanes passing frequency. An amplitude of 0.43 kPa was observed at the normalized frequency of 0.70 which is related to the difference between the runner frequency and the vortex

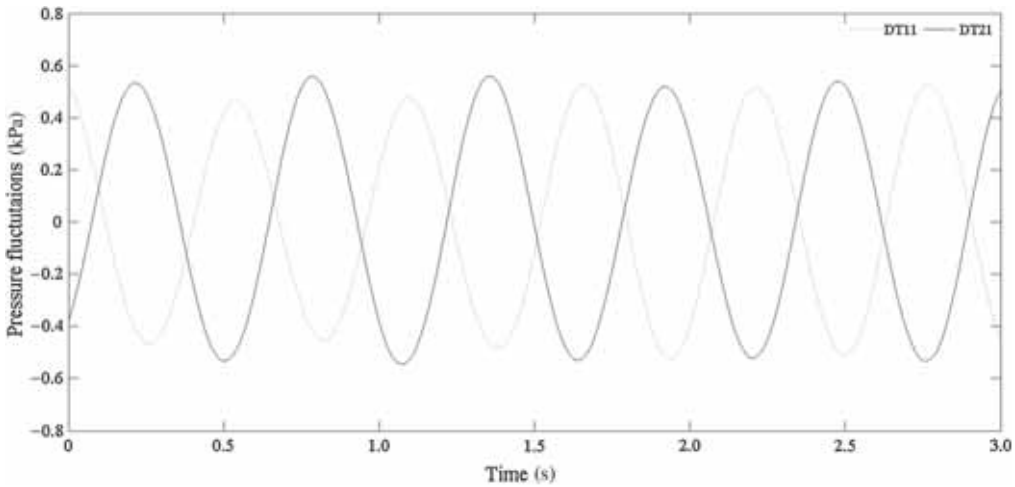

Figure 7. Experimental filtered pressure fluctuations at the vortex rope frequency in the draft tube at DT11 and DT21.

breakdown frequency. This difference is due to the same rotational direction of the rotating vortex rope (RVR) as that of the runner. In case of high load, the direction of RVR will be opposite to the runner rotational direction. The amplitude of this frequency was decreasing from the runner outlet to the runner inlet, i.e., the maximum amplitude was observed at P71. Pressure signals acquired by the draft tube sensors DT11 and DT21 showed that the maximum amplitude occurred at two specific normalized frequencies, 0.29 and 30. The frequency of 0.29 corresponded to the vortex breakdown in the draft tube. The second harmonic of the vortex breakdown frequency was also observed at both of the draft tube sensors. The frequency of 30, corresponding to the blades passing frequency, was also found in the draft tube at DT11 and DT21. The observed amplitudes were 0.55 and 0.10 kPa at both the sensors for the vortex breakdown and RSI frequencies, respectively.

Further analysis of the pressure time signals of DT11 and DT21 sensors has been carried out at the vortex breakdown frequency as shown in figure 7. It is seen that the signals are nearly 180° out-of-phase to each other indicating the presence of a RVR in the draft tube. The pressure fluctuations of the vortex rope frequency at DT11 and DT21 are out-of-phase because the vortex moves around the center line of the draft tube and travels to the second sensor after a phase difference of 180°. The pressure time signal for a time length of 3 s is presented in figure 7 which is equivalent to the runner rotation of 5.50 cycles. The maximum amplitude of the frequency was 0.55 kPa at both the locations. The pressure waves developing due to the vortex breakdown are observed in the entire domain of the model Francis turbine extending from draft tube inlet to the inlet pipe location PTX2 (see figure 6).

It is seen from figure 7 that the signals from DT11 and DT21 sensors are not exactly 180° out-of-phase. To further investigate this, these signals were decomposed using the procedure given by Bosioc *et al* [17]. The synchronous and asynchronous components of the two signals DT11 and DT21 are determined as below

$$\frac{(A_1 + A_2)}{2} = \text{Synchronous component (Plunging) of the pressure signal} \quad (6)$$

$$\frac{(A_1 - A_2)}{2} = \text{Asynchronous component (Rotating) of the pressure signal} \quad (7)$$

where A_1 and A_2 are the pressure signals from the two sensors DT11 and DT21 respectively.

A plot of the plunging and the rotating components of the vortex rope are shown in figure 8. The sinusoidal variation of the plunging and the rotating component of the vortex rope show that the latter is dominating over the former. In the runner, only the rotating component was observed. This may be explained by the damping of the pressure fluctuations as they propagate upstream and the initial low amplitude of the plunging component.

4. Conclusions

The present work contributes to the understanding of the hydrodynamics of a high head model Francis turbine operating at 50% of rated load. Transient pressure measurements showed unsteadiness of the pressure in all the regions of the turbine. The average pressure in the turbine showed continuous drop in the pressure till the end of splitter blade, and a small pressure recovery in the draft tube. Due to rotor–stator interaction, significant pressure fluctuations were observed in the vaneless space and draft tube at blade pass frequency whereas that corresponds to guide vane pass frequency in the runner. However, the pressure fluctuations in the draft tube were found to be

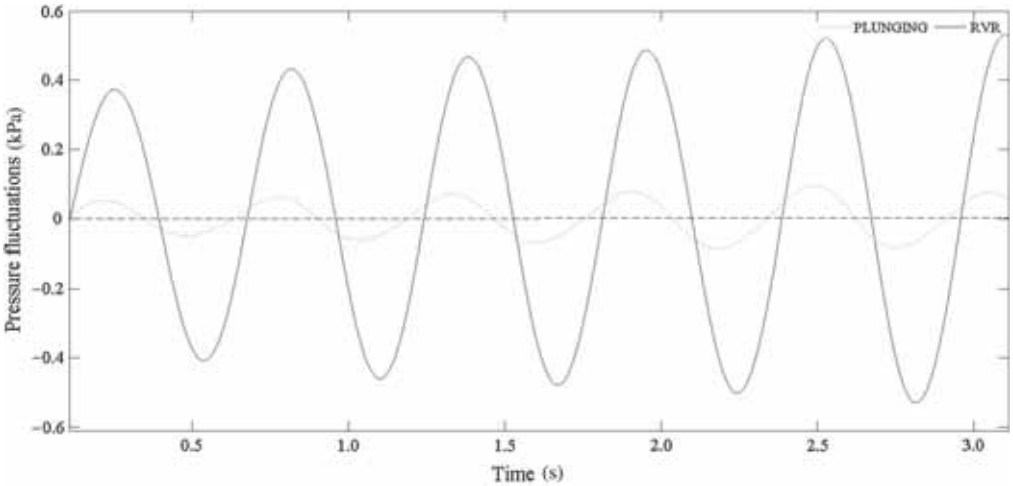

Figure 8. Experimental pressure fluctuation of the signal DT11 and DT22 at low discharge for the rotating vortex rope and plunging components.

dominated by the vortex breakdown frequency and it was observed as 1/3 of the runner frequency. Further analysis of the pressure signals of the draft tube showed dominance of the rotating component over the plunging component. The pressure fluctuations traveled upstream; the effect of runner vane pass frequency and vortex rope frequency was observed till short distance upstream of the turbine inlet.

Abbreviations

BEP	best efficiency point
RSI	rotor stator interactions
RVR	rotating vortex rope
FFT	fast Fourier transform
Δp	pressure difference across the turbine (Pa)
$\tilde{p}$	acquired pressure signal (kPa)
$\bar{p}$	mean pressure (kPa)
p^*	fluctuating pressure (kPa)
t	time (s)
f	observed frequency (Hz)
f_n	runner rotational frequency (Hz)
f*	normalized frequency (–)
F_{c1}	upper cut-off frequency
F_{c2}	lower cut-off frequency
H_{LP1}	low-pass filter
H_{BS}	bandpass filter
g	9.821465 (m s^{-2}), as tested and measured at NTNU
n_{ED}	speed factor $[-]$, $n_{ED} = \frac{nD}{\sqrt{gH_M}}$
n_s	specific speed $[-], n_s = \frac{\left(n_P \cdot \frac{\pi}{180}\right)\sqrt{Q_P}}{(2 \cdot g \cdot H_P)^{\frac{3}{4}}}$
p	pressure (kPa); harmonic order (1,2,….)
Q	flow rate (m^3 s^{-1})
q_{ED}	discharge factor $[-], q_{ED} = \frac{Q}{D^2\sqrt{gH_M}}$
X	discrete quantity
$\overline{X}$	average value
N	sampling length
λ	wavelength (m)
α	angular vane/blade position (°)
δ	uncertainty (%)

References

[1] Chirag T, Cervantes M, Bhupendra G and Dahlhaug O G 2013 Experimental and numerical studies for a high head Francis turbine at several operating points. *J. Fluids Eng.* 135(11): 111102

[2] Antonsen O 2007 *Unsteady flow in wicket gate and runner with focus on static and dynamic load runner*. Doctoral thesis. NTNU, Norway

[3] Breivik S 2011 *CFD-analysis of a runner and draft tube in a Francis turbine*. Master thesis, EPT-M-2011-56, NTNU, Norway

[4] Keck H and Sick M 2008 Thirty years of numerical flow simulation in hydraulic turbomachines. *ActaMech* 201: 211–229

[5] Nicolet C 2007 *Hydroacoustic modelling and numerical simulation of unsteady operation of hydroelectric systems*. Doctoral thesis. École Polytechnique Fédérale de Lausanne

[6] Brekke H 2010 A review on oscillatory problems in Francis turbine. *New trends in technologies: Devices, computer, communication and industrial systems*. ISBN-978-953-307-212-8, pp 217–232 (Chapter 12).

[7] Staubli T, Senn F and Sallaberger M 2008 Instability of pump-turbines during start-up in turbine mode. *The 15th annual conference HYDRO 2008*, 6–8 October, Ljubljana, Slovenia

[8] Hasmatuchi V, Farhat M, Roth S, Botero F and Avellan F 2011 Experimental evidence of rotating stall in a pump-turbine at off-design conditions in generating mode. *J. Fluids Eng.* 133: 051101-1-8

[9] Xiao Y, Wang Z and Yan Z 2010 Experimental and numerical analysis of blade channel vortices in a Francis turbine runner. *Int. J. Comput.-Aided Eng. Softw.* 28(2): 154–171

[10] Zobeiri A, Kukny J L, Farhat M and Avellan F 2006 Pump-turbine rotor-stator interactions in generating mode: Pressure fluctuation in distributer channel. In: *23rd IAHR Symposium*. Yokohama

[11] Arpe J, Nicolet C and Avellan F 2009 Experimental evidence of hydroacoustic pressure waves in a Francis turbine elbow draft tube for low discharge conditions. *J. Fluids Eng.* 131: 081102-1-9

[12] Ciocan G D, Iliescu M S and Vu C T, Nennemann B and Avellan F 2007 Experimental study and numerical simulation of the FLINDT draft tube rotating vortex. *J. Fluids Eng.* 129: 146–158

[13] Nicolet C, Herou J-J, Greiveldinger B, Allenbach P, Simond J-J and Avellan F 2006 Methodology for risk assessment of part load resonance in Francis turbine power plant. *IAHR International Meeting of the WorkGroup on Cavitation and Dynamic Problems in Hydraulic Machinery and Systems Barcelona*, 28–30

[14] Cervantes M J, Andersson U and Lovgren H M 2010 Turbine-99 unsteady simulations-validations. *Earth and Environment Science,* vol. 12, 012014, pp. 1–10

[15] Haban V, Koutnik J and Pochyly F 2002 1-D mathematical model of high-frequency pressure fluctuations induced by RSI including an influence of fluid second viscosity. In: *21st IAHR Symposium*, Lausanne

[16] Fisher R, Powell C, Franke G, Seidel U and Koutnik J 2004 Contributions to improved understanding of the dynamic behavior of pump turbine and use thereof in dynamic design. In: *22nd IAHR Symposium*, Stockholm

[17] Bosioc A L, Resiga R S, Muntean S and Tanasa C 2012 Unsteady pressure analysis of a swirling flow with vortex rope and axial water injection in a discharge cone. *J. Fluids Eng.* 134: 081104-1

[18] IEC 60193: 1999–2011 *Hydraulic turbines, storage pumps and pump-turbines – Model acceptance tests*. International Electrotechnical Commission, Geneva, Switzerland

[19] IEC 60041: 1991–2011 *Field acceptance tests to determine the hydraulic performance of hydraulic turbines, storage pumps and pump-turbines*. Third edition. International Electrotechnical Commission, Geneva, Switzerland

[20] Houde S, Iliescu M S, Fraser R, Lemay S, Ciocan G D and Deschenes C 2011 Experimental and numerical analysis of the cavitating part load vortex dynamics of low-head hydraulic turbines. In: *Proceedings of ASME-JSME-KSME joint Fluids Engineering Conference*, July 24–29, 2011, Hamamatsu, and Shizuoka, Japan